Optimum Droop Parameter Settings of Islanded Microgrids With Renewable Energy Resources

Morad Mohamed Abdelmageed Abdelaziz, *Student Member*, *IEEE*, Hany E. Farag, *Member*, *IEEE*, and Ehab F. El-Saadany, *Senior Member*, *IEEE*

***Abstract*—Droop control is a key strategy for operating distributed generation (DG) islanded systems, i.e., islanded microgrids (IMGs). The droop parameter settings of the DG units can significantly impact the ability of an IMG to feed its demand. This paper proposes a new probabilistic algorithm for determining the optimum choice for such droop settings for the individual DG units in a distribution network in cases when a microgrid central controller is unavailable. The proposed algorithm adopts a constraint hierarchy approach to enhance the operation of IMGs by satisfying the operational constraints of the system and expanding its loading margin. The new algorithm takes into consideration the variety of possible IMG configurations that can be initiated in a distribution network (multi-microgrids), the uncertainty and variability associated with the output power of renewable DG units as well as the variability of the load, and the special features and operational philosophy associated with droop-controlled IMG systems. Simulation studies show that the proposed algorithm can facilitate the successful implementation of the IMG concept by reducing the customer interruptions and enhancing the IMGs' loadability margins.**

***Index Terms*—Droop control, hierarchy constraints, islanded microgrid (IMG), renewable resources, voltage regulation and security.**

NOMENCLATURE

A. Acronyms

DFIG	Doubly fed induction generator.
DG	Distributed generation.
DNO	Distribution network operator.
IID	Island isolation device.
IMG	Islanded microgrid.
LIB	Limit-induced bifurcation.
MCS	Monte Carlo simulation.
MGCC	Microgrid central controller.
PCC	Point of common coupling.
PDF	Probability density function.
SNB	Saddle node bifurcation.

B. Functions

$eC_p(.)$	Error function of the preferred constraint level p in a given constraint hierarchy C.
$F^{(\mathrm{is,st})}(.)$	Power flow equations of islanded microgrid "is" at state "st."
$f(.)$	Distribution probability of wind speed.

C. Indices

i, j, k	Index of system buses.
is	Index of islanded microgrids.
ℓ	Index of system loading points.
p	Index of preference level in a constraint hierarchy.
st	Index of states.

D. Parameters

n_{bus}	Number of system buses.
n_{levels}	Number of constraint hierarchy levels of preference.
n_{MG}	Number of possible islanded microgrids in the system under study.
$n_{\mathrm{states}}^{(\mathrm{is})}$	Number of islanded microgrid "is" states.
P_{Li}, Q_{Li}	Active and reactive nominal load power at bus i, respectively.
$S_{Gi,\max}$	Apparent power generation capacity at bus i.
$S_{\mathrm{loss\ \&\ spare}}^{(\mathrm{is,st})}$	Apparent power loss and spare capacity requirements for islanded microgrid "is" operating at state "st."
$v_{\mathrm{st,min}}$, $v_{\mathrm{st,max}}$	Wind speed limits of state "st."
$\Gamma^{(\mathrm{is,st})}$	Parameter indicating the priority of islanded microgrid "is" at state "st."
$\Gamma_i^{(\mathrm{is,st})}$	Parameter indicating the priority of load point i when operating in islanded microgrid "is" at state "st."
$\lambda_{\mathrm{ub}}^{(\mathrm{is,st})}$	Upper bound on the loading factor of islanded microgrid "is" at state "st."
$\rho_{\mathrm{st}}^G, \rho_{\mathrm{st}}^L, \rho_{\mathrm{st}}$	Probability of generation, load, and combined states, respectively.

E. Sets

B	Set of all system buses.
$B^{(\mathrm{is})}$	Set of all buses in islanded microgrid "is."
B_{droop}	Set of all droop-controlled buses in the system.
$B_{\mathrm{droop}}^{(\mathrm{is})}$	Set of all droop-controlled buses in islanded microgrid "is."
C_0	Set of mandatory constraints in a given constraint hierarchy C.
C_p	Set of preferred constraints of p preference level in a given constraint hierarchy C.
N_{st}^G, N_{st}^L, N_{st}	Set of all possible generation, load, and combined generation-load states, respectively.

Manuscript received June 06, 2013; revised September 21, 2013 and October 21, 2013; accepted November 24, 2013. Date of publication January 10, 2014; date of current version March 18, 2014.

M. M. A. Abdelaziz and E. F. El-Saadany are with the Electrical and Computer Engineering Department, University of Waterloo, Waterloo, ON N2L 3G1, Canada (e-mail: m3abdelm@uwaterloo.ca; ehab@uwaterloo.ca).

H. E. Farag is with the Department of Electrical Engineering and Computer Science, York University, Toronto, ON M3J 1P3, Canada (e-mail: hefarag@cse.yorku.ca).

Color versions of one or more of the figures in this paper are available online at http://ieeexplore.ieee.org.

Digital Object Identifier 10.1109/TSTE.2013.2293201

1949-3029 © 2014 IEEE. Personal use is permitted, but republication/redistribution requires IEEE permission.
See http://www.ieee.org/publications_standards/publications/rights/index.html for more information.

Authorized licensed use limited to: UNIV OF MIAMI LIB. Downloaded on May 27,2022 at 21:50:44 UTC from IEEE Xplore. Restrictions apply.

Z_0 Set of all admissible solutions to a constraint hierarchy.

Z_p Set of all constraint hierarchy solutions that satisfy constraints up to and including level p.

F. Variables

$h^{(\mathrm{is,st})}$ Vector of state variables of islanded microgrid "is," operating at state "st" including system frequency, voltage magnitudes, and angles.

$I_{ik}^{(\mathrm{is,st})}$ Magnitude of the current flowing in the line between the buses i and k when operating in islanded microgrid "is" at state "st."

m_{pi}, n_{qi} Active and reactive power static-droop gains for droop-controlled DG unit at bus i, respectively.

P_{Gi}, Q_{Gi} Generated active and reactive power at bus i, respectively.

$P_{Gi,\max}$, $Q_{Gi,\max}$ Active and reactive power generation capacities at bus i, respectively.

$|V_i|^*, \omega_i^*$ No-load output voltage magnitude and frequency of droop-controlled DG unit at bus i, respectively.

$|V_i|, \delta_i$ Voltage magnitude and angle at bus i, respectively.

$\Delta V_i^{(\mathrm{is,st})}$ Binary variable indicating the voltage regulation status of load point i when operating in islanded microgrid "is" at state "st."

x Unknown droop setting variables for all droop-controlled DG units in the system.

x_j Unknown droop setting variables for the droop-controlled DG unit at bus j.

$|Y_{ik}|, \theta_{ik}$ Frequency-dependent Y-bus admittance magnitude and angle, respectively.

z Solution of constraint hierarchy.

ω Steady-state frequency of droop-controlled DG units output voltages.

$\lambda^{(\mathrm{is,st},\ell)}$ Loading factor of islanded microgrid "is" at state "st" for loading point ℓ.

I. Introduction

DRIVEN by the urgent need to develop cleaner and more efficient, reliable, resilient, and responsive power grids, the energy sector is currently moving toward an era of smart grids [1]. The main pillar of a smart grid setup is the evolution from a vertically integrated electric power network to a decentralized one that enables interactions among customers, network operators, and power producers. In response to smart grid initiatives, the distribution systems are undergoing a major transition to active distribution systems with a high penetration of distributed and renewable energy resources [2]. Active distribution systems will be clustered into a new set of management layers based on a microgrid structure, which is considered as the building block of future active distribution systems [3], [4]. A typical microgrid configuration is formed of a cluster of loads and distributed generation (DG) units connected to a distribution network [5]–[7]. The microgrids will provide several benefits for the utilities and customers, the most important of which is the increased reliability for microgrid customers. During upstream disturbances, the microgrids can be isolated from the main grid in order to maintain the continuity of electric power service. The majority of DG units in microgrids are interfaced through a voltage–source converter coupled with a passive output filter [8], [9]. In an islanded microgrid (IMG) operating mode, these DG units are responsible for maintaining the system voltage and frequency while sharing the load demand. The literature includes descriptions of two proposed operational schemes for controlling such DG units operating in IMGs: centralized and droop control schemes [9], [10]. Dependent on the availability of high-bandwidth communication links, a centralized control scheme is usually found to be 1) impractical and costly because it requires the distribution of high-bandwidth dynamic sharing signals among the DG units that form the IMG and 2) unreliable due to the single point of failure associated with the use of a centralized control approach. These limitations can be overcome through a decentralized droop control scheme that depends on locally measured signals without high-bandwidth communication links for achieving appropriate sharing of the load demand while still controlling the voltage and frequency of the IMG.

In IMGs, droop-controlled DG units are controlled so that they mimic the droop characteristics of synchronous generators operating in parallel. The settings of the droop characteristics for the individual DG units thus affect their steady-state active and reactive power generation. Conventionally, the droop characteristics are designed so that the DG units forming the IMG share the load demand in proportion to their rated capacity [11]. Generally, such conventional droop settings are capable of providing nearly exact active power sharing among DG units in IMGs. Nonetheless, these settings might not satisfy other system operational requirements, where the reactive power sharing between the DG units is inexact and dependent on the system parameters; i.e., mismatches in the power line impedances can lead to high levels of circulating reactive power. Also, conventional droop settings can ensure voltage regulation at the DG units' points of common coupling (PCCs); however, a voltage violation might occur at some load points due to voltage drops along the feeders, and previous work [12] has shown that the voltage and reactive power constraints have a significant impact on the successful operation of IMGs. A final factor is that the conventional droop settings fail to take into consideration the system's maximum loadability which is a key consideration in the case of IMGs because the system is fed from a group of small DG units with limited capacities.

In the literature, several researchers have proposed methods for the optimal selection of DG units' droop parameter settings in order to enhance the droop-controlled IMG operation [13]–[18]. However, these methods presuppose the existence of a microgrid central controller (MGCC) and a noncritical low-bandwidth communication infrastructure to complement the droop control scheme. In this paradigm, the optimization of the IMG operation is performed centrally by a higher level coordinated management function at the MGCC. Using periodic measurements of the IMG generation and loads, the MGCC updates the DG unit droop settings (i.e., characteristics) in order to optimally dispatch the different DG units in the IMG.

Nevertheless, the operation of IMGs without an MGCC is still a viable solution in a number of scenarios [12], the most critical

Authorized licensed use limited to: UNIV OF MIAMI LIB. Downloaded on May 27,2022 at 21:50:44 UTC from IEEE Xplore. Restrictions apply.

of which occurs when the microgrid is intended to operate only in emergency conditions during inadvertent events in the upstream network; i.e., events that might initiate the transition to islanded mode of operation are unscheduled [3]. The expected short time spans of such IMG operation might not motivate the installation of an MGCC and its associated communication infrastructure. In these scenarios, no periodic updating of the DG unit droop settings will take place, and they must, therefore, be predesigned offline for a possible operational planning horizon within which the IMGs might be initiated. Such droop settings design should 1) be capable of satisfying the operational constraints of the system in all operating conditions based on the consideration of the uncertainty and variability associated with the renewable DG output power and load variability; 2) take into consideration the different microgrid configurations that can be created within a typical distribution network, in which the same settings of a DG unit must enable its operation in different possible islands; 3) ensure the ability of the IMG to feed the maximum possible demand by enhancing the voltage instability proximity index, calculated over all the states in which the islanded system may exist.

Based on these considerations, this paper proposes a new probabilistic algorithm for the optimum choice of droop settings for individual DG units in a distribution network when an MGCC is unavailable. The proposed algorithm adopts a constraint hierarchy approach to enhance the operation of IMGs by satisfying the operational constraints of the system and by expanding its loading margin. The algorithm accounts for the variety of possible microgrid configurations that can be initiated in a distribution network, the special features and operational philosophy associated with droop-controlled IMG systems, and the stochastic nature of the system generation and loads. It can, thus, be an effective and powerful tool for helping distribution network operators (DNOs) select the optimum droop settings for the DG units in the distribution network in order to enable the successful operation of IMGs either in the absence of an MGCC or when an MGCC fails to operate. The remainder of this paper is organized as follows. Section II presents the droop-controlled IMG structure and the steady-state model used for its representation. In Section III, a probabilistic load-generation model that incorporates the stochastic nature of droop-controlled IMG components is introduced. The formulation of the problem of optimally choosing the droop settings for the individual DG units is explained in Section IV. Section V provides the simulation results for a variety of case studies that demonstrate the effectiveness and significance of the proposed approach. Section VI concludes the paper and summarizes the main contributions.

II. IMG Structure and Steady-State Modeling

In a distribution network that includes the DG units, a variety of IMG configurations can be created and can be identified based on the zone associated with the devices that permit the islanding of the microgrid from the distribution network [i.e., island isolation devices (IIDs)] [3]. Such devices can be the circuit breakers or automatic re-closers. Fig. 1 depicts the examples of microgrid configurations that can be initiated in a distribution network. As shown, the distribution network is configured into a set of microgrids, each of which is basically a group of

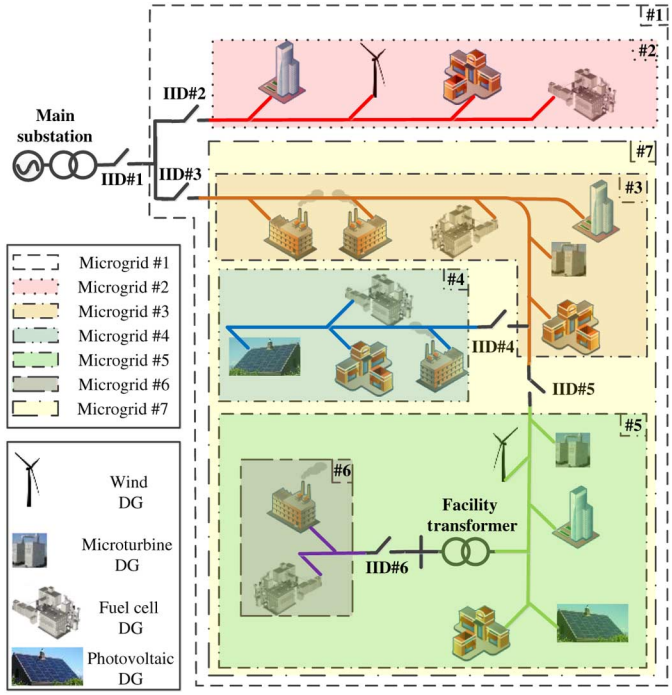

Fig. 1. Structure of a distribution network considering the microgrids.

components (e.g., lines, DG units, loads, and protection devices) with an IID at its entry. It is worth noting that a DG unit or load point can belong to different possible microgrid configurations depending on the fault and the IID location. For example, as shown in Fig. 1, load points downstream of IID #6 can fall within IMG #1, #5, #6, or #7, depending on the location of the fault that initiates the islanded operation. Based on this structure and with the absence of an MGCC, one IMG will be initiated to include all downstream microgrids if a fault occurs in its upstream system. For instance, Microgrid #6 will be islanded if a fault occurs upstream of it in the electrical region defined by Microgrid #5. However, Microgrid #5 will be islanded if a fault occurs in the electrical region defined by Microgrid #3.

In a droop control structure, active power sharing is achieved by drooping the frequency of the output voltage of the DG unit as the active power generated by the DG unit increases. Similarly, the magnitude of the output voltage of the DG unit is drooped as the reactive power generated by the DG unit increases [6]. Accordingly, for a droop-controlled DG unit connected to the ith bus, the DG output voltage frequency ω and magnitude $|V_i|$ can be given as follows:

$$\omega = \omega_i^* - m_{pi} P_{Gi} \tag{1}$$

$$|V_i| = |V_i|^* - n_{qi} Q_{Gi} \tag{2}$$

where ω_i^* and $|V_i|^*$ are the DG unit output voltage frequency and magnitude at no-load, m_{pi} and n_{qi} are the active and reactive power static-droop gains, and P_{Gi} and Q_{Gi} are the injected active and reactive power by the DG unit, respectively. From (1) and (2), it can be seen that the droop characteristics provide a measure of negative proportional feedback that controls the active and reactive power sharing of the system. The negative feedback relation in (1) also ensures that all of the DG units

Authorized licensed use limited to: UNIV OF MIAMI LIB. Downloaded on May 27,2022 at 21:50:44 UTC from IEEE Xplore. Restrictions apply.

are producing voltages with the same steady-state angular frequency, i.e., system steady-state angular frequency [9], [10]. It is worth noting that the transient behavior of a droop-controlled DG unit can be adapted to modify the dynamic stability of the IMG system by replacing the negative proportional feedback in (1) and (2) with active and reactive power dynamic compensation, respectively. However, irrespective of the compensators design used, the dc gain of such compensators always represents the static-droop gains (i.e., m_{pi} and n_{qi}) that control the steady-state operating point of the system [10], [19]. Starting with a prespecified set of static-droop gains to implement a particular steady-state response, the design of dynamic compensators for shaping the transient response of the DG units can be achieved as a second step without affecting the steady-state solution required for the system [10], [19]. An algorithm for scheduling the transfer functions of the active and reactive power compensators starting from different static-droop gains has been proposed in the previous work by the third author [10]. Accordingly, the steady-state behavior of droop-controlled DG units can be represented using only (1) and (2).

The overall steady-state behavior of droop-controlled IMGs is modeled by a set of power flow equations. Unlike conventional power flow formulations, power flow equations for a droop-controlled IMG have the following characteristics: 1) the power generated by droop-controlled DG units is determined based on the DG unit droop characteristics set by (1) and (2) and cannot be prespecified prior to the solution of the power flow equations and 2) a droop-controlled IMG has no slack bus capable of maintaining a constant system frequency, as such the steady-state frequency of the system is not prespecified and is one of the power flow variables. The set of power flow equations that reflect the special philosophy of operation of a droop-controlled IMG can, therefore, be formulated as follows, for each droop bus i, there are two mismatch equations:

$$\frac{1}{m_{pi}}(\omega_i^* - \omega) - P_{Li} = \sum_{k\in B}(|V_i||V_k||Y_{ik}|\cos(\theta_{ik}+\delta_k-\delta_i)) \quad (3)$$

$$\frac{1}{n_{qi}}(|V_i|^* - |V_i|) - Q_{Li} = -\sum_{k\in B}(|V_i||V_k||Y_{ik}|\sin(\theta_{ik}+\delta_k-\delta_i)) \quad (4)$$

where P_{Li} and Q_{Li} are the active and reactive load power at bus i, Y_{ik} and θ_{ij} are the frequency-dependent Y-bus admittance magnitude and angle, respectively, and δ_i is the voltage angle at bus i. The dispatchable DG units operating in droop-controlled mode provide the energy buffering required for enabling the islanded operation [20], [21]. In constrast, renewable energy resources are locally controlled in order to track their maximum power operating point and are, therefore, represented as PQ buses in the IMG model [12]. The power mismatch equations for PQ nodes are similar to conventional power flow formulations [11]. Consequently, the number of mismatch equations that describe the power flow in an islanded condition is made up of $2\times n_{\text{bus}}$-equations comprising the $2\times n_{\text{bus}}$-unknown variables to be calculated. The angle of an arbitrary bus is set to zero so that it can be taken as the system reference [11].

In this work, the conventional droop equations expressed by (1) and (2) have been used in compliance with IEEE standard 1547.4 for DG islanded systems. These characteristics are usually justified based on the assumption that the output impedance of the droop-controlled DG unit is mainly inductive due to the coupling inductor used at the DG interface converter output, the X/R ratio of the network feeders, or the use of a virtual inductive output impedance [11], [19]. However, it is worth noting that, in some cases, the output impedance of the droop-controlled DG unit is highly resistive due to the absence of a coupling inductor, to predominately resistive line impedances, or to the use of virtual resistive output impedance. In such cases, the roles of the P/Q droops expressed by (1) and (2) are exchanged and $P-V$ and $Q-\omega$ droop characteristics are used [22]. In [23] and [24], it was also shown that, in several practical applications, a DG unit output impedance can be complex, in which active and reactive power sharing cannot be completely decoupled. $P-V-\omega$ and $Q-V-\omega$ droop characteristics are then used [23], [24]. These droop characteristics, for either resistive or complex converter output impedances, can easily be implemented in the proposed algorithm by replacing (1) and (2) with the respective $P-V/Q-\omega$ or $P-V-\omega/Q-V-\omega$ droop equations [22]–[24].

III. Probabilistic IMG Model

Accurate droop setting for IMG systems should take into consideration the stochastic nature of both the generation and the loads. This section explains the analytical development of a combined generation load model for describing all possible system states and their respective probabilities [25]. Assuming that the probabilities of the generation states in the operational planning horizon $\rho_{\text{st}}^G\{N_{\text{st}}^G\}$ are independent of the probabilities of the load states $\rho_{\text{st}}^L\{N_{\text{st}}^L\}$, the probabilities of states $\rho_{\text{st}}\{N_{\text{st}}\}$ describing different possible combinations of generation and load states in an IMG can be obtained by convolving their respective probabilities as follows:

$$\rho_{\text{st}}\{N_{\text{st}}\} = \rho_{\text{st}}^G\{N_{\text{st}}^G\}^*\rho_{\text{st}}^L\{N_{\text{st}}^L\} \quad (5)$$

where $\{N_{\text{st}}^G\}$ is the set of all possible generation states, $\{N_{\text{st}}^L\}$ is the set of all possible load states, and $\{N_{\text{st}}\}$ is the set of all possible IMG states. Based on (5), the generation load model for an IMG can be obtained by listing all possible combinations of generation output power states and load states. Similarly, different generation states are composed by convolving generation state probabilities based on the state model of each type of DG unit. For two DG units G_1 and G_2, with different state models, the model of the combined generation states can be obtained as follows:

$$\rho_{\text{st}}^G\{N_{\text{st}}^G\} = \rho_{\text{st}}^{G_1}\{N_{\text{st}}^{G_1}\}^*\rho_{\text{st}}^{G_2}\{N_{\text{st}}^{G_2}\} \quad (6)$$

where $\{N_{\text{st}}^{G_1}\}$ and $\{N_{\text{st}}^{G_2}\}$ are the set of all possible generation states for the first and second DG units, respectively.

Generally, the generation states model for variable power DG units is calculated by dividing the continuous probability distribution function (PDF) into several states. For example, the generation states model of wind-based DG units can be extracted

Authorized licensed use limited to: UNIV OF MIAMI LIB. Downloaded on May 27,2022 at 21:50:44 UTC from IEEE Xplore. Restrictions apply.

by dividing the wind speed PDF into several states with a step of 1 m/s. The probability of a wind state "st" can then be calculated as follows:

$$\rho_{\mathrm{st}}^{\mathrm{wind}}(s) = \int_{v_{\mathrm{st,min}}}^{v_{\mathrm{st,max}}} f(v) \cdot dv \tag{7}$$

where $f(v)$ is the distribution probability of wind speed and $v_{\mathrm{st,min}}$ and $v_{\mathrm{st,max}}$ are the wind speed limits of state "st," respectively. Similar approaches can be used for other variable power sources [25]. The studies in [25] revealed no significant differences between the results obtained using this analytical approach and those obtained using Monte Carlo simulation (MCS).

IV. Proposed Optimal Droop Parameter Settings

The choice of droop settings for the operation of different droop-controlled DG units in the event that an IMG is initiated can significantly impact the capability of such an island to successfully feed its loads. This section presents the formulation of the problem of optimally choosing the droop settings for such DG units in a given distribution network in order first to satisfy the operational constraints of the system and second to enhance the voltage security margins. The droop setting variables to be determined can be given as

$$x = \{x_j | \forall j \in B_{\mathrm{droop}}\} \tag{8}$$

where

$$x_j = \lfloor \omega_j^*, m_{pj}, |V_j^*|, n_{qj} \rfloor \tag{9}$$

and B_{droop} is the set of all droop-controlled buses in the system. The proposed algorithm takes into consideration 1) the unavailability of an MGCC and its associated communication infrastructure, 2) the uncertainty and variability associated with the system loads and renewable generation, 3) the different possible IMG configurations that can be initiated in the distribution network, and 4) the special features and operational philosophy of the droop-controlled IMG systems. Fig. 2 shows a flowchart of the proposed probabilistic algorithm. As can be seen, the algorithm is divided into two stages, as detailed in the following sections.

A. Stage 1: Supply Adequacy Evaluation

Irrespective of the droop settings in place, an island can be successful if and only if there is enough generation to match the total demand of the island. The first stage in the proposed algorithm is, therefore, to determine the set of states with sufficient generation to meet its respective demand for each possible IMG (i.e., the set of admissible microgrid states). Based on the generation-load model described in Section III, the necessary condition for an IMG "is" operating at a given state "st" to be admissible is given as follows:

$$\sum_{i \in B^{(\mathrm{is})}} S_{Gi,\max}^{(\mathrm{is,st})} \geq \sqrt{\left(\sum_{i \in B^{(\mathrm{is})}} P_{Li}^{(\mathrm{is,st})}\right)^2 + \left(\sum_{i \in B^{(\mathrm{is})}} Q_{Li}^{(\mathrm{is,st})}\right)^2} + S_{\mathrm{loss\&spare}}^{(\mathrm{is,st})} \tag{10}$$

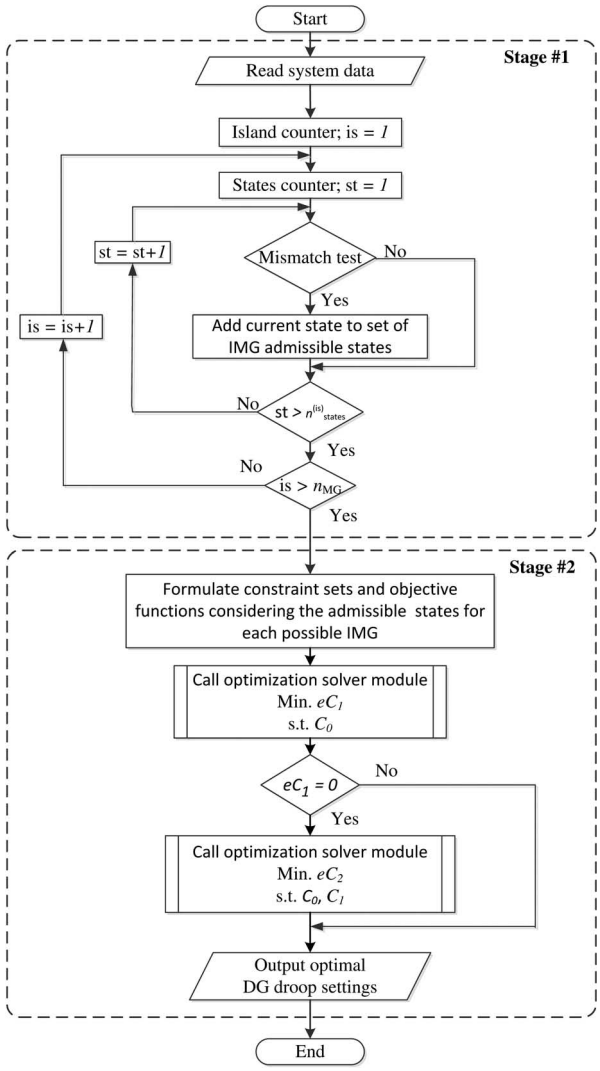

Fig. 2. Flowchart of the proposed algorithm.

where "is" is the index of IMGs, "st" is the index of state, $B^{(\mathrm{is})}$ is the set of all buses in IMG "is," $S_{Gi,\max}^{(\mathrm{is,st})}$ is the apparent power generation capacity at bus i when operating in IMG "is" at state "st," and $S_{\mathrm{loss\&spare}}^{(\mathrm{is,st})}$ is the apparent power loss and spare capacity requirements for IMG "is" operating at state "st." The condition in (10) shows that an IMG state is considered admissible if enough apparent power generation is available to match the island total load, power loss, and spare capacity requirements. The spare capacity defined in this stage is intended to account for the ability of the microgrid to respond to unexpected and sudden increases in its local power demand (i.e., spinning reserve) [12], [13]. Different options can affect the definition of spare capacity for an IMG. One option is to define the spare capacity to represent a specific percentage of the load demand. In this work, the spare capacity was arbitrarily defined as 5% of the total demand in the microgrid [13]. It is worth mentioning that in this stage, the power loss in the island feeders is considered to be 5% of the microgrid demand [12], [25].

B. Stage 2: Constraint Hierarchy Approach

Although the choice of droop characteristics cannot lead to any reduction in the IMG customers' interruption caused by the

Authorized licensed use limited to: UNIV OF MIAMI LIB. Downloaded on May 27,2022 at 21:50:44 UTC from IEEE Xplore. Restrictions apply.

IMG unsuccessful operation due to the generation-to-load mismatch, a proper setting of droop characteristics can minimize the customers' interruption resulting from the violation of voltage constraints. In this stage, the droop settings are, thus, optimally selected to minimize customer interruption due to voltage regulation and security issues taking into consideration all admissible states of each possible IMG. The problem is divided into two steps: the first is to satisfy the operational voltage regulation constraints at the different system buses and the second is to increase the voltage security margin. In this work, the theory of constraint hierarchy is applied as a means of performing these steps.

The theory of constraint hierarchy was originally defined in [26]. A constraint hierarchy consists of a multi-set of labeled constraints, each identified as either mandatory or preferred. The mandatory constraints must hold for any valuation of the system-free variables. The preferred constraints should be satisfied as fully as possible. An arbitrary number of preference levels are permitted for the preferred constraints, with each successive level being weaker than its predecessor. For a given constraint hierarchy C, C_0 is the set of mandatory constraints in C with strength 0 always reserved for the mandatory constraints. For n_{levels} levels of preferences, C_p with $p \in \{1, 2, \ldots, n_{\text{levels}}\}$ denotes the sets of preferred constraints. A solution z to a given constraint hierarchy C is a specific valuation of the system-free variables. A solution that satisfies all the mandatory constraints in the hierarchy is called an admissible solution. Z_0 is the set of all possible admissible solutions to C

$$Z_0 = \{z | \forall c_0 \in C_0, c_0(z) \text{holds}\}. \tag{11}$$

The set of preferred constraints that each admissible solution in Z_0 also satisfies, respecting their strength level, is used for the selection of the best solution from Z_0. A best solution is one compared to which no better solution exists. To determine the best solution in Z_0, an error function $eC_p(z)$ is defined for each of the preferred constraint levels. This function returns a non-negative real number that indicates how closely C_p is satisfied for a valuation z, such that $eC_p(z) = 0$ if and only if $C_p(z)$ is satisfied. A solution z_a is better than another solution z_b, if, for each level l through some level $p-1$, $eC_l(z_a)$ is equal to $eC_l(z_b)$ and also at level p, it is strictly less

$$\begin{aligned} z_a \text{is better than } z_b \equiv \exists p > 0 | (eC_l(z_a) = eC_l(z_b)\, \forall l \\ \in \{1, \ldots, p-1\}) \wedge (eC_p(z_a) < eC_p(z_b)). \end{aligned} \tag{12}$$

The constraint hierarchy is built level by level from the constraints of the highest preference in the hierarchy down to those with lower ones. For example, if all C_p constraints can be satisfied, then C_{p+1} (weaker than C_p) will be added to the constraint hierarchy, following which the satisfaction of C_{p+1} can then be checked in turn.

Fig. 3 shows the establishment of the constraint hierarchy for the problem under study. The outer space shown in Fig. 3 contains the set of solutions Z_0 that satisfy the bounds of the droop settings and the hard constraints of the system at each admissible state for each possible IMG (i.e., power flow equations as well as generation and line capacity limits). Each solution in Z_0 has a specific ability to minimize the IMG customer interruptions that result from the violation of voltage regulation constraints. An inner subspace Z_1 might thus be defined as the solution domain in which all solutions satisfy the voltage regulation constraints (i.e., no customer interruptions due to the voltage regulation problem). If Z_1 exists, then another sub-space Z_2 is defined so that the system voltage security constraints are satisfied (i.e., $Z_2 \subseteq Z_1 \subseteq Z_0$).

Sustained voltage levels that fall outside the specified voltage regulation constraints result in the unsatisfactory operation of utilization equipment. The operational status of individual load points, in particular, is determined based on the designed under-voltage/overvoltage protection schemes. However, even if the load points do not have their own protection devices, due to their unsatisfactory operation in the case of a voltage violation, they should be accounted for as interrupted loads [12]. It is worth noting here that consideration of the voltage regulation constraints in the C_0 level might result in an infeasible problem if any load point, at any admissible state of any possible IMG, is subject to a voltage violation. In this work, the voltage regulation constraint has, therefore, been defined as the first level of the hierarchy constraint problem. In this level, the proposed algorithm attempts to satisfy the voltage regulation constraints by minimizing the number of voltage violation incidents in the possible IMGs, as given by the error function eC_1. The best solution for this constraint level can hence be found by solving the following optimization problem:

$$\text{Min.} eC_1 \equiv \sum_{\text{is}}^{n_{\text{MG}}} \left(\sum_{\text{st}}^{n_{\text{states}}^{(\text{is})}} \left(\sum_{i \in B^{(\text{is})}} \Gamma_i^{(\text{is,st})} \times \Delta V_i^{(\text{is,st})} \right) \right) \tag{13a}$$

subject to (13b)–(13f), shown at the bottom of the page. $\forall \text{is} \in \{1, 2, \ldots, n_{\text{MG}}\}$, $\forall \text{st} \in \{1, 2, \ldots, n_{\text{states}}^{(\text{is})}\}$, $\forall j \in B_{\text{droop}}^{(\text{is})}$,

$$C_0 \begin{cases} F^{(\text{is,st})}(\boldsymbol{h}^{(\text{is,st})}, x) = 0 & \text{(13b)} \\ x_{\text{lb}} \le x \le x_{\text{ub}} & \text{(13c)} \\ I_{ik}^{\text{lb}} \le I_{ik}^{(\text{is,st})} \le I_{ik}^{\text{ub}} & \text{(13d)} \\ 0 \le S_{Gj,\max}^{(\text{is,st})} - P_{Gj}^{(\text{is,st})} \perp \frac{1}{x_j(2)} \times (x_j(1) - \omega^{(\text{is,st})}) - P_{Gj}^{(\text{is,st})} \ge 0 & \text{(13e)} \\ 0 \le \sqrt{(S_{Gj,\max}^{(\text{is,st})})^2 - (P_{Gj}^{(\text{is,st})})^2} - Q_{Gj}^{(\text{is,st})} \perp \frac{1}{x_j(4)} \times (x_j(3) - |V_j|^{(\text{is,st})}) - Q_{Gj}^{(\text{is,st})} \ge 0 & \text{(13f)} \end{cases}$$

Authorized licensed use limited to: UNIV OF MIAMI LIB. Downloaded on May 27,2022 at 21:50:44 UTC from IEEE Xplore. Restrictions apply.

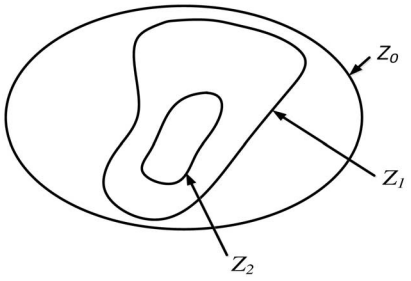

Fig. 3. Conceptual illustration of the constraint hierarchy theory.

and $\forall i, k \in B^{(\mathrm{is})}$ where n_{MG} is the number of possible IMGs in the system under study, $n_{\mathrm{states}}^{(\mathrm{is})}$ is the number of IMG "is" states, $\Gamma_i^{(\mathrm{is,st})}$ is a parameter indicating the priority of load point i when operating in IMG "is" at state "st," $\boldsymbol{h}^{(\mathrm{is,st})}$ is the vector of state variables of IMG "is" operating at state "st" including system frequency, voltage magnitudes, and angles, $I_{ik}^{(\mathrm{is,st})}$ is the magnitude of the current flowing in the line between the buses i and k when operating in IMG "is" at state "st," $B_{\mathrm{droop}}^{(\mathrm{is})}$ is the set of all droop-controlled buses in IMG "is," and $\Delta V_i^{(\mathrm{is,st})}$ is a binary variable indicating the voltage regulation status of load point i when operating in IMG "is" at state "st." ΔV_i equals zero when the voltage at the load point is within the voltage regulation constraints and equals one otherwise. The variables in the minimization problem given by (13a) are the unknown DG units' droop parameter settings and the power flow variables for each admissible state of each possible IMG. The equality constraints in (13b) represent the set of IMG power flow equations given by (1)–(4) for each admissible state of each possible IMG. The upper and lower bounds on the droop parameter settings given by (13c) are determined based on the allowable voltage and frequency regulations at the DG units' PCCs [9]. Equations (13d)–(13f) represent the line currents and the capacity constraints of the droop-controlled DG units for each admissible state of each possible IMG. For an IMG "is" operating at a given state "st," the active and reactive power generation of the droop-controlled DG units follow the droop relations given in (1) and (2) up till the DG units' maximum active and reactive power generation limits, $P_{Gj,\max}^{(\mathrm{is,st})}$ and $Q_{Gj,\max}$, respectively. Beyond $P_{Gj,\max}^{(\mathrm{is,st})}$, the active power generation of the DG units is not permitted to follow the droop relation given by (1), and the DG is transformed so that it injects a constant amount of active power set at the violated limit (i.e., $P_{Gj,\max}^{(\mathrm{is,st})}$). Similarly, beyond $Q_{Gj,\max}^{(\mathrm{is,st})}$, the reactive power generation of the DG units is not allowed to follow the droop relation given by (2), and the DG is transformed so that it injects a constant amount of reactive power set at the violated limit (i.e., $Q_{Gj,\max}^{(\mathrm{is,st})}$). The relationships governing the jth droop-controlled DG unit active and reactive power generation capabilities can be given as [27]

$$P_{Gj,\max}^{(\mathrm{is,st})} = S_{Gj,\max}^{(\mathrm{is,st})} \tag{14}$$

$$Q_{Gj,\max}^{(\mathrm{is,st})} = \sqrt{(S_{Gj,\max}^{(\mathrm{is,st})})^2 - (P_{Gj}^{(\mathrm{is,st})})^2}. \tag{15}$$

In the proposed problem formulation, to model the behavior of DG units as they reach their maximum generation capability, a set of nonlinear complementary constraints have been adopted: (13e) and (13f). The nonlinear complementary constraint problem, as defined in [28] and [29], is to find the vector $\partial \in \Re^n$ such that for the given mappings $\gamma(\boldsymbol{\partial}) : \Re^n \to \Re^n$ and $\beta(\boldsymbol{\partial}) : \Re^n \to \Re^n$

$$\gamma(\boldsymbol{\partial}) \geq 0, \quad \beta(\boldsymbol{\partial}) \geq 0, \quad \gamma(\boldsymbol{\partial}) \times \beta(\boldsymbol{\partial}) = 0. \tag{16}$$

With the notation "$\perp$" indicating complement, (16) can be written as

$$0 \leq \gamma(\boldsymbol{\partial}) \perp \beta(\boldsymbol{\partial}) \geq 0. \tag{17}$$

The complementary constraints in (13e) and (13f) mean that the active and reactive power generation of the DG unit are either following the droop characteristics given by (1) and (2) or set at the DG limits given by (14) and (15): $P_{Gj,\max}^{(\mathrm{is,st})}$ and $Q_{Gj,\max}^{(\mathrm{is,st})}$.

The voltage security problem is associated with the increase in system demand beyond specific limits, which leads to the disappearance of the system equilibrium point [29]–[31]. The overall operational limit of the microgrid can be closely associated with the voltage stability of the network. Hence, the incorporation of the voltage collapse criterion in the selection of the droop settings is important for maximizing the distance from the operating point to the point of voltage collapse, which in turn increases the robustness of the system with respect to withstanding possible contingencies. The voltage security margin quantifies the proximity of an IMG state to the point of voltage collapse. The point at which the steady-state solution for the system disappears (i.e., the point of voltage collapse) is known as the static bifurcation point. For a linearly increasing load, with $\lambda \in \Re$ representing a scalar load factor, assuming an increase in the generation capacity to match the load increase, the disappearance of the steady-state solution for the system with an increasing λ can be related to the appearance of a singularity in the Jacobian matrix of the power flow equations describing the droop-controlled IMG. This type of bifurcation is known as a saddle-node bifurcation (SNB). Moreover, considering the operational limits and the capacity limits of the DG units in the IMG, a reduced static voltage stability margin might result. In this case, the disappearance of the system equilibrium can occur instantaneously, with a sudden jump to instability as the capacity limit of system equipment or an operational limit is reached. This type of bifurcation is known as a limit-induced bifurcation (LIB).

Accordingly, in this work, the second level of the constraint hierarchy attempts to maximize the voltage security margin through the minimizing of the difference between the IMG maximum loading margin and its respective upper bounds, given by the error function eC_2. The best solution for this constraint level can hence be found by solving the following optimization problem:

$$\mathrm{Min}.eC_2 \equiv \sum_{\mathrm{is}}^{n_{\mathrm{MG}}} \left(\sum_{\mathrm{st}}^{n_{\mathrm{states}}^{(\mathrm{is})}} \Gamma^{(\mathrm{is,st})} \times (\lambda_{\mathrm{ub}}^{(\mathrm{is,st})} - \lambda^{(\mathrm{is,st},m)}) \right) \tag{18a}$$

Authorized licensed use limited to: UNIV OF MIAMI LIB. Downloaded on May 27,2022 at 21:50:44 UTC from IEEE Xplore. Restrictions apply.

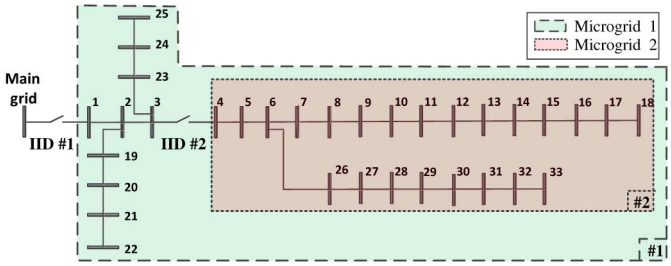

Fig. 4. 33-Bus distribution test system [32].

subject to (18b)–(18g), shown at the bottom of the page. $\forall \text{is} \in \{1, 2, \ldots, n_{\text{MG}}\}$, $\forall \text{st} \in \{1, 2, \ldots, n_{\text{states}}^{(is)}\}$, $\forall \ell \in \{c, m\}$, $\forall j \in B_{\text{droop}}^{(\text{is})}$, and $\forall i, k \in B^{(\text{is})}$ where ℓ is the index of system loading points, c and m indicate the current and maximum loading points, respectively, $\Gamma^{(\text{is,st})}$ is a parameter indicating the priority of IMG "is" at state "st," $\lambda^{(\text{is,st},\ell)}$ is the loading factor of IMG "is" at state "st" for loading point ℓ, and $\lambda_{\text{ub}}^{(\text{is,st})}$ is the upper bound on the loading factor of IMG "is" at state "st," and is given by

$$\lambda_{\text{ub}}^{(\text{is,st})} = \sum_{i \in B^{(\text{is})}} S_{Gi,\max}^{(\text{is,st})} \Bigg/ \left(\sqrt{\left(\sum_{i \in B^{(\text{is})}} P_{Li}^{(\text{is,st})} \right)^2 + \left(\sum_{i \in B^{(\text{is})}} Q_{Li}^{(\text{is,st})} \right)^2} \right). \tag{19}$$

V. Case Studies

The proposed probabilistic approach was coded in a MATLAB environment. The optimization problems in (13) and (19) were solved using an interior point method for mathematical programs with complementary constraints [29]. A 33-bus system [32] was used in the case studies. Fig. 4 shows a single-line diagram of the test system. The feeder parameters and nominal power of the load are given in [32]. Four dispatchable DG units and two wind-based DG units were allocated to feed the system in IMG operation mode. The ratings, locations, and types of the DG units are listed in Table I. Two possible IMGs can be formed by the two IIDs shown in Fig. 4. The upper and lower limits on the variation in node voltage were taken as 1.05 and 0.95 p.u., respectively. A maximum frequency variation of ± 0.005 p.u. was considered in the case studies investigated. For this work, the load was divided into 10 states using the clustering technique developed in [33]. The wind-speed profile was estimated from the previous 3 years of historical data, based on which the 12-state model developed in [25] was used, including the generated power and probabilities for each wind turbine. The set of load states was combined with the set of wind power states for each wind turbine in order to extract the generation-load model of each IMG [25]. Two case studies were considered as a means of evaluating the relevance of the proposed algorithm. The first case study is an examination of the operation of an islanded system with conventional droop settings. The second case study is an investigation of the operation of the system when the droop settings are optimally selected according to the proposed algorithm.

TABLE I
DG Locations, Ratings, and Control Modes in the 33-Bus Test System ($S_{\text{base}} = 1$ MVA)

DG #	Bus #	S_{Gmax} (p.u.)	Type	Mode
1	04	3.00	Dispatchable	Droop
2	08	0.50	Dispatchable	Droop
3	18	0.75	DFIG wind	PQ-0.95 PF lead
4	22	1.50	Dispatchable	Droop
5	24	0.50	DFIG wind	PQ-0.95 PF lead
6	25	1.00	Dispatchable	Droop

A. Case Study 1: Conventional Droop Settings

In case study 1, the static-droop gains of the DG units are designed in order to share the load demand of the IMG proportionally with the rated capacity of the DG units [9]; V^* and ω^* are selected arbitrarily in order to maintain adequate power-quality levels, in terms of maintaining the frequency and voltage within their respective specified operating limits. Such conventional droop settings are capable of providing proper frequency regulation and nearly exact active power sharing among DG units in IMGs [11]. Using the conventional droop settings, the IMG power flow algorithm given by (1)–(4) is solved for all admissible IMG states (with $\omega^* = 1.0$ p.u. at different values of V^*). Fig. 5(a) and (b) shows the minimum and maximum voltages, respectively, that can occur at the different system buses considering all possible IMGs that can be initiated to include such buses as well as all possible generation and load states of such islands, with different arbitrary values of V^*. These figures show that the choice of V^* can significantly affect IMG voltage regulation. An arbitrary choice of V^* can lead to undervoltage and/or overvoltage problems. Further, when all DG units have the same V^* setting, the change in such a value cannot guarantee effective voltage regulation for all possible operating states. In contrast,

$$C_0 \begin{cases} F^{(\text{is,st},\ell)}\left(\boldsymbol{h}^{(\text{is,st},\ell)}, x, \lambda^{(\text{is,st},\ell)}\right) = 0 & \text{(18b)} \\ x_{\text{lb}} \le x \le x_{\text{ub}} & \text{(18c)} \\ I_{ik}^{\text{lb}} \le I_{ik}^{(\text{is,st},\ell)} \le I_{ik}^{\text{ub}} & \text{(18d)} \\ 0 \le S_{Gj,\max}^{(\text{is,st},\ell)} - P_{Gj}^{(\text{is,st},\ell)} \perp \frac{1}{x_j(2)} \times \left(x_j(1) - \omega^{(\text{is,st},\ell)}\right) - P_{Gj}^{(\text{is,st},\ell)} \ge 0 & \text{(18e)} \\ 0 \le \sqrt{\left(S_{Gj,\max}^{(\text{is,st},\ell)}\right)^2 - \left(P_{Gj}^{(\text{is,st},\ell)}\right)^2} - Q_{Gj}^{(\text{is,st},\ell)} \perp \frac{1}{x_j(4)} \times \left(x_j(3) - |V_j|^{(\text{is,st},\ell)}\right) - Q_{Gj}^{(\text{is,st},\ell)} \ge 0 & \text{(18f)} \end{cases}$$

$$C_1 \left\{ |V_i|^{\text{lb}} \le |V_i|^{(\text{is,st},\ell)} \le |V_i|^{\text{ub}} \right. \tag{18g}$$

Authorized licensed use limited to: UNIV OF MIAMI LIB. Downloaded on May 27,2022 at 21:50:44 UTC from IEEE Xplore. Restrictions apply.

TABLE II
OPTIMAL DROOP SETTINGS OBTAINED IN CASE STUDY 2

DG #	Scenario 1				Scenario 2				Scenario 3			
	V^*	w^*	m_p	n_q	V^*	w^*	m_p	n_q	V^*	w^*	m_p	n_q
1	1.024	1.0018	1.67E–03	1.67E–02	1.016	1.0009	7.29E-04	1.65E–05	1.011	1.0001	3.59E–04	1.30E–05
2	1.017	1.0016	1.00E–02	1.00E–01	1.016	1.0008	4.03E-03	6.17E–02	1.011	1.0000	1.88E–03	1.86E–02
4	1.016	1.0014	3.33E–03	3.33E–02	1.040	1.0009	1.22E-03	3.21E–02	1.011	1.0000	2.05E–03	2.57E–02
6	1.017	1.0014	5.00E–03	5.00E–02	1.018	1.0010	2.47E-03	5.09E–04	1.013	1.0001	1.02E–03	5.32E–05

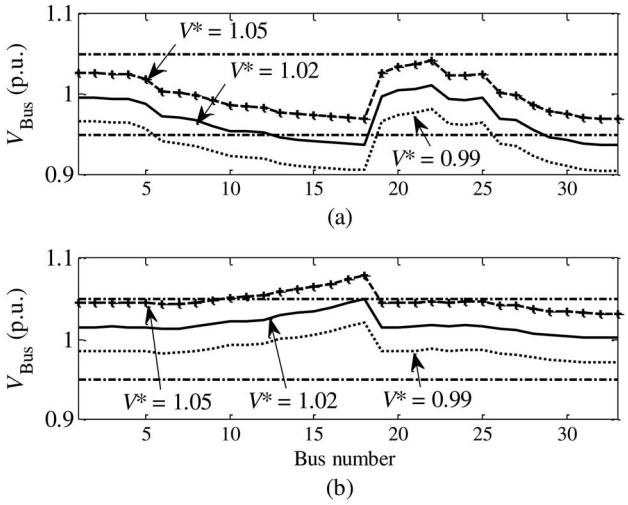

Fig. 5. Case study 1: (a) minimum and (b) maximum voltage magnitudes for all buses at different values of V^* using conventional droop settings considering all admissible system states and all possible IMGs. (In this case study, all droop-controlled DG units operate at the same V^* setting).

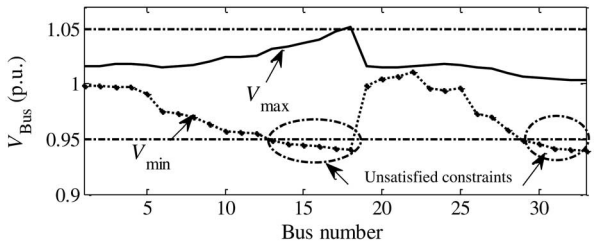

Fig. 6. Minimum and maximum voltage magnitudes with the settings obtained in the first scenario of case study 2.

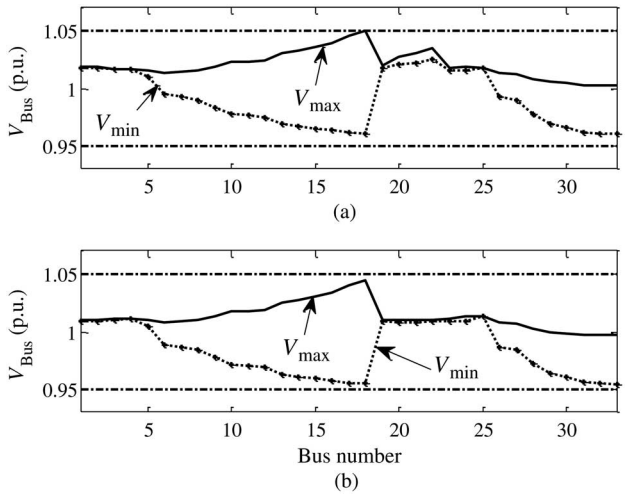

Fig. 7. Minimum and maximum voltage magnitudes with the settings obtained in the (a) second and (b) third scenarios of case study 2.

arbitrary selection of different V^* settings for different DG units is not an easy task, given the presence of intermittent renewable power sources and the fact that the voltage profile does not follow a consistent descending trend toward the feeder terminal. Avoiding such improper voltage regulation renders the arbitrary choice of different V^* values for the DG units cumbersome, and they need, thus, to be selected optimally.

B. Case Study 2: Proposed Optimal Droop Settings

In this case study, three possible scenarios are considered. In the first scenario, the proposed algorithm is applied for optimally selecting the no-load nominal voltage and frequency droop settings (i.e., V^* and ω^*) for the different droop-controlled DG units. In this scenario, the static-droop gains are not optimized and are kept proportional to the capacities of the DG units as in case study 1. Table II lists the optimal V^* and ω^* settings for droop-based DG units obtained in this scenario. Fig. 6 shows the minimum and maximum voltages based on the consideration of all admissible system states and all possible microgrids when operating with the optimal settings obtained in this scenario. The results obtained in the first scenario show that the optimal choice of V^* and ω^* cannot guarantee the satisfaction of the system voltage operational constraints given in C_1. Based on the proposed two-level hierarchy constraint algorithm, because the C_1 constraints are not satisfied, the results obtained in this scenario are optimal only in terms of error function eC_1. Consequently, the values obtained for V^* and ω^* are not based on consideration of the voltage instability proximity expressed by the error function eC_2.

In the second scenario, the proposed two-level hierarchy constraint algorithm optimally selects all the droop settings for the different DG units in the system (i.e., V^*, ω^*, m_p, and n_q). The third scenario investigates the importance of including consideration of the maximum loadability of the system in the optimal selection of the system droop parameters. Accordingly, in the third scenario, the proposed algorithm is thus limited to consideration of only the C_0 and C_1 levels in the constraint hierarchy. Table II shows the settings obtained in the second and third scenarios. Here, it is worth noting that the valuation of the optimization variables obtained in the third scenario is not unique and that the other variable valuations can satisfy the problem constraints. Fig. 7(a) and (b) shows the minimum and maximum voltages that can occur at the different system buses in the second and third scenarios, respectively, considering all admissible system states and all possible IMGs that can be initiated to

Authorized licensed use limited to: UNIV OF MIAMI LIB. Downloaded on May 27,2022 at 21:50:44 UTC from IEEE Xplore. Restrictions apply.

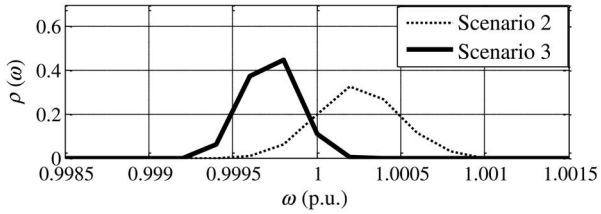

Fig. 8. PDFs of the system frequency with the settings obtained in the second and third scenarios of case study 2.

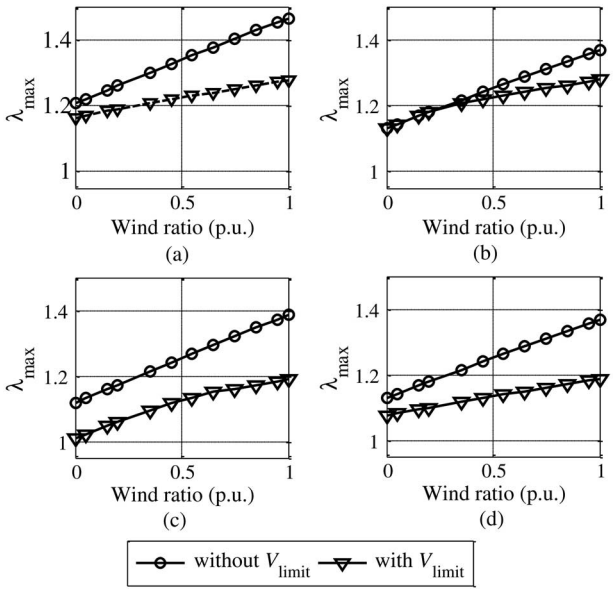

Fig. 9. Maximum loadability with settings obtained in scenarios 2 and 3 at different wind power ratios: (a) IMG #1, scenario 2; (b) IMG #2, scenario 2; (c) IMG #1, scenario 3; and (d) IMG #2, scenario 3.

include such buses. As can be seen in Fig. 7(a) and (b), the droop settings obtained in the second and third scenarios are both capable of satisfying the operational voltage constraints for the different system states given by C_1.

Fig. 8 shows the PDFs of the system frequency for the second and third scenarios. As shown in this figure, the lower and upper bounds imposed on the static-droop coefficients by (13c) and (18c) guarantee the maintenance of the system frequency within the allowable deviation tolerance. It is worth noting that similar bounds imposed on the reactive power static-droop gain coefficients can ensure proper voltage regulation only at the PCC. Voltage drops across the distribution feeders may still lead to voltage violations at different system buses. Fig. 9(a)–(d) shows the maximum system loadability at different wind-power ratios (ratio of the available wind power over the rated wind power capacity) in the second and third scenarios for IMG #1 and IMG #2. Two sets of results are plotted in each figure: those labeled "without V_{limit}" represent the maximum system loadability when no bus voltage limits are enforced at the maximum loading point and the results labeled "with V_{limit}" represent the maximum system loadability when the bus voltage limits are enforced at the maximum loading point. For both sets of results, the line capacity limits and the active and reactive power limits of the DG units are always enforced. As one would expect, the presence of bus

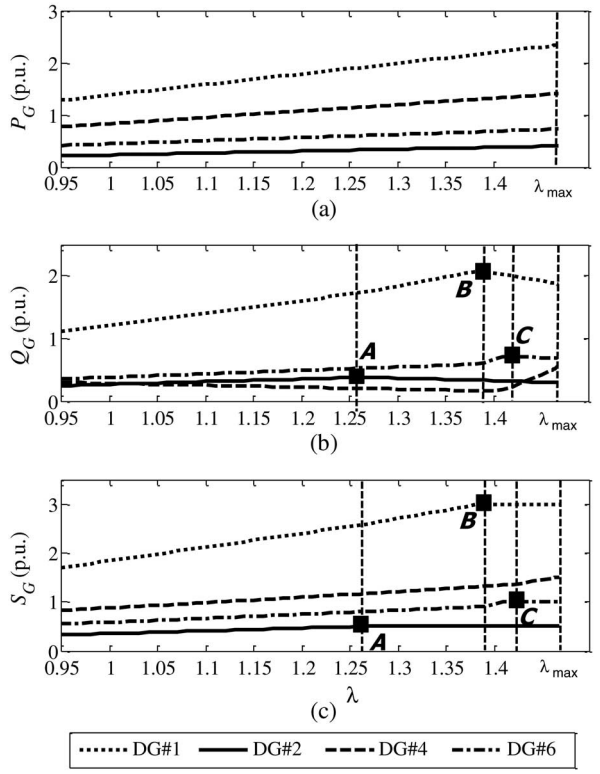

Fig. 10. DG units' generation as λ increases with the settings obtained in scenario 2 for IMG #1: (a) active power, (b) reactive power, and (c) apparent power.

voltage limits at the maximum loading point reduces the loadability margin of the islanded systems. These figures also demonstrate that the maximum loadability achieved with the settings obtained in the second scenario is significantly higher than that obtained with the settings from the third scenario. This, in turn, indicates the importance of including consideration of the maximum loadability of the system, as given by C_2 in the proposed two-level hierarchy constraint algorithm. However, Fig. 9(b) and (d) shows that the maximum loadability of IMG #2 "without V_{limit}" with the settings obtained from the second and third scenarios almost coincide along the wind-power ratio trajectory. This particular observation can be attributed to the presence of a dominant DG unit (DG #1) in IMG #2, which results in the optimization of the droop settings having a reduced impact on the maximum loadability of the system.

Figs. 10 and 11 show the DG units' generation as IMG #1 loading increases for the settings obtained in the second and third scenarios, respectively. As shown in Figs. 10(a) and 11(a), the increase in active power generation with the increase in the system loading is governed by the droop relation given in (1), for all the droop-controlled DG units in the system. In Fig. 10(b) and (c), three system loading levels have been highlighted on the generation plots. At these loading levels, points "A," "B," and "C" correspond to the point at which maximum generation capacity is reached by DG #2, DG #1, and DG #6, respectively. For each of these points, as the DG unit reaches its maximum apparent power capacity, the reactive power production switches from being governed by the droop control equation given by (2) to being governed by the available capacity as denoted by (15).

Authorized licensed use limited to: UNIV OF MIAMI LIB. Downloaded on May 27,2022 at 21:50:44 UTC from IEEE Xplore. Restrictions apply.

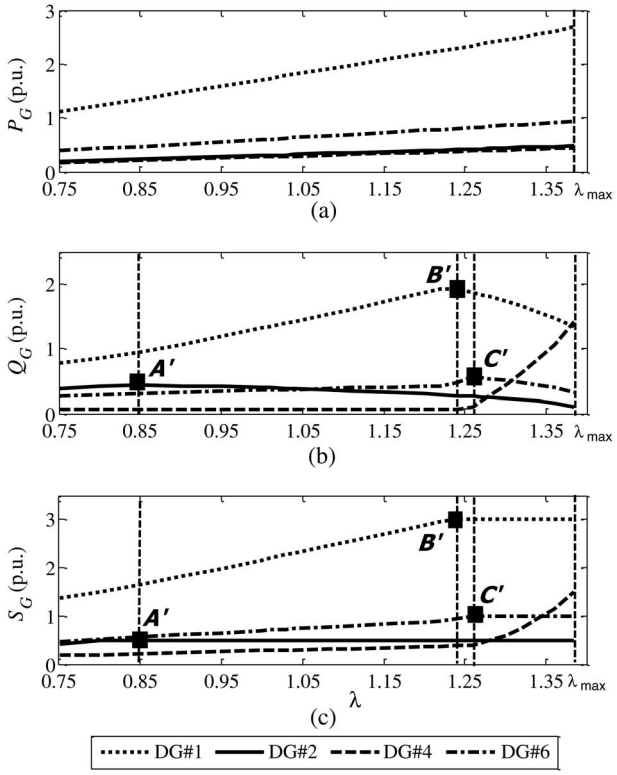

Fig. 11. DG units' generation as λ increases with the settings obtained in scenario 3 for IMG #1: (a) active power, (b) reactive power, and (c) apparent power.

This change, in turn, affects the reactive power generated by other DG units. For example, Fig. 10(c) shows that at point "B," DG #1 and DG #2 are producing their maximum apparent power. A further increase in the loading factor from point "B" to point "C," hence, results in a decrease in the reactive power production of DG #1 and DG #2 in order to preserve their active power-sharing capability. The increase in the reactive power demands resulting from the loading factor increase and the reduction in reactive power production by DG #1 and DG #2 is, therefore, shared between DG #4 and #6. Given the respective values of the reactive power static-droop gains of these DG units, it can be seen that DG #4 feeds a significantly higher portion of the reactive power demand increase. In Fig. 11(b) and (c), similar system loading levels are highlighted. Comparing the results obtained in Figs. 10 and 11, it can be seen that the load sharing obtained by the settings from the second scenario allows for higher system loadability as compared with the settings from the third scenario. These results further demonstrate the ability of the proposed two-level hierarchy constraint algorithm to achieve higher system loadability.

The impact of voltage and generation capacity constraints on the maximum system loadability was analyzed: Fig. 12 shows the voltage–magnitude profile as a function of the system loadability (PV curve) for the most remote bus in IMG #1 (bus #33) with the settings obtained in the second scenario. Point "X" shows the maximum system loadability when both the voltage and generation capacity constraints are considered, point "Y" shows the maximum system loadability when only the generation capacity constraints are considered, and point "Z" represents the maximum system loadability when the system is

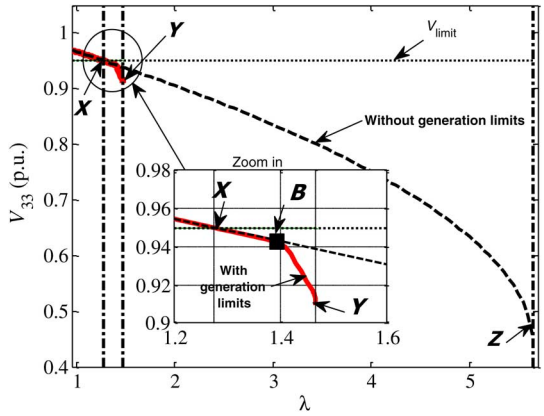

Fig. 12. Voltage at bus 33 as a function of λ with the settings obtained in scenario 2 for IMG #1.

unconstrained. Points "X" and "Y" are LIB points, whereas point "Z" is an SNB point. The rapid descent in the voltage–magnitude from point "B" to point "Y," also depicted in Fig. 12, could be associated with the transfer of reactive power support from DG #1 to the remoter DG #4 and DG #6, as DG #1 reaches its maximum capacity at point "B." Fig. 12 shows that the voltage and generation capacity constraints significantly reduce the loadability margin of the IMG.

VI. Conclusion

This paper proposed a new probabilistic algorithm for the offline selection of DG units' droop parameter settings for a possible operational planning horizon within which IMGs might be initiated. The proposed algorithm applies a detailed IMG model along with a probabilistic analytical technique to account for special IMG features and the variability in system generation and demand. The algorithm also includes consideration of different possible IMG configurations that can be initiated in the distribution network. A constraint hierarchy approach is incorporated as a means of minimizing the IMG customer interruption, first by satisfying the operational system constraints and second by enhancing the voltage security margins. Simulation studies have been carried out to demonstrate the effectiveness of the proposed algorithm. The results reveal that the proposed algorithm is capable of significantly reducing the IMG customer interruptions and enhancing the IMGs' voltage security margins. The findings also show that an effective selection of droop parameters settings will facilitate the successful implementation of the IMG concept in the distribution networks.

References

[1] K. Moslehi and R. Kumar, "A reliability perspective of the smart grid," *IEEE Trans. Smart Grid*, vol. 1, no. 1, pp. 57–64, Jun. 2010.

[2] L. F. Ochoa, C. J. Dent, and G. P. Harrison, "Distribution network capacity assessment: Variable DG and active networks," *IEEE Trans. Power Syst.*, vol. 25, no. 1, pp. 87–95, Feb. 2010.

[3] *IEEE Guide for Design, Operation, and Integration of Distributed Resource Island Systems With Electric Power Systems*, IEEE Standard 15474, Jul. 2011.

[4] H. Kanchev, D. Lu, F. Colas, V. Lazarov, and B. Francois, "Energy management and operational planning of a microgrid with a PV-based active generator for smart grid applications," *IEEE Trans. Ind. Electron.*, vol. 58, no. 10, pp. 4583–4592, Oct. 2011.

Authorized licensed use limited to: UNIV OF MIAMI LIB. Downloaded on May 27,2022 at 21:50:44 UTC from IEEE Xplore. Restrictions apply.

[5] B. Belvedere, M. Bianchi, A. Borghetti, C. A. Nucci, M. Paolone, and A. Peretto, "A microcontroller-based power management system for standalone microgrids with hybrid power supply," *IEEE Trans. Sustain. Energy*, vol. 3, no. 3, pp. 422–431, Jul. 2012.
[6] M. Fazeli, G. M. Asher, C. Klumpner, Y. Liangzhong, and M. Bazargan, "Novel integration of wind generator-energy storage systems within microgrids," *IEEE Trans. Smart Grid*, vol. 3, no. 2, pp. 728–737, Jun. 2012.
[7] T. Logenthiran, D. Srinivasan, A. M. Khambadkone, and H. Nwe Aung, "Multiagent system for real-time operation of a microgrid in real-time digital simulator," *IEEE Trans. Smart Grid*, vol. 3, no. 2, pp. 925–933, Jun. 2012.
[8] F. Blaabjerg, R. Teodorescu, M. Liserre, and A. V. Timbus, "Overview of control and grid synchronization for distributed power generation systems," *IEEE Trans. Ind. Electron.*, vol. 53, no. 5, pp. 1398–1409, Oct. 2006.
[9] N. Pogaku, M. Prodanovic, and T. C. Green, "Modeling, analysis and testing of autonomous operation of an inverter-based microgrid," *IEEE Trans. Power Electron.*, vol. 22, no. 2, pp. 613–625, Mar. 2007.
[10] Y. Mohamed and E. F. El-Saadany, "Adaptive decentralized droop controller to preserve power sharing stability of paralleled inverters in distributed generation microgrids," *IEEE Trans. Power Electron.*, vol. 23, no. 6, pp. 2806–2816, Nov. 2008.
[11] M. M. Abdelaziz, H. E. Farag, E. F. El-Saadany, and Y. A.-R. Mohamed, "A novel and generalized three-phase power flow algorithm for islanded microgrids using a Newton trust region method," *IEEE Trans. Power Syst.*, vol. 28, no. 1, pp. 190–201, Feb. 2013.
[12] H. E. Farag, M. M. A. Abdelaziz, and E. F. El-Saadany, "Voltage and reactive power impacts on successful operation of islanded microgrids," *IEEE Trans. Power Syst.*, vol. 28, no. 2, pp. 1716–1727, May 2013.
[13] C. A. Hernandez-Aramburo, T. C. Green, and N. Mugniot, "Fuel consumption minimization of a microgrid," *IEEE Trans. Ind. Appl.*, vol. 41, no. 3, pp. 673–681, May 2005.
[14] E. Barklund, N. Pogaku, M. Prodanovic, C. Hernandez-Aramburo, and T. C. Green, "Energy management in autonomous microgrid using stability-constrained droop control of inverters," *IEEE Trans. Power Electron.*, vol. 23, no. 5, pp. 2346–2352, Sep. 2008.
[15] S. A. Pourmousavi, M. H. Nehrir, C. M. Colson, and C. Wang, "Real-time energy management of a stand-alone hybrid wind-microturbine energy system using particle swarm optimization," *IEEE Trans. Sustain. Energy*, vol. 1, no. 1, pp. 193–201, Oct. 2010.
[16] P. H. Divshali, S. H. Hosseinian, and M. Abedi, "A novel multi-stage fuel cost minimization in a VSC-based microgrid considering stability, frequency, and voltage constraints," *IEEE Trans. Power Syst.*, vol. 28, no. 2, pp. 931–939, May 2013.
[17] S. Conti, R. Nicolosi, S. A. Rizzo, and H. H. Zeineldin, "Optimal dispatching of distributed generators and storage systems for MV islanded microgrids," *IEEE Trans. Power Del.*, vol. 27, no. 3, pp. 1243–1251, Jul. 2012.
[18] A. Basu, A. Bhattacharya, S. Chowdhury, and S. P. Chowdhury, "Planned scheduling for economic power sharing in a CHP-based microgrid," *IEEE Trans. Power Syst.*, vol. 27, no. 1, pp. 30–38, Feb. 2012.
[19] J. M. Guerrero, J. C. Vasquez, J. Matas, L. G. de Vicuna, and M. Castilla, "Hierarchical control of droop-controlled ac and dc microgrids—A general approach towards standardization," *IEEE Trans. Ind. Electron.*, vol. 58, no. 1, pp. 158–172, Jan. 2011.
[20] G. Díaz, C. González-Morán, and C. Viescas, "Operating point of islanded microgrids consisting of conventional doubly fed induction generators and distributed supporting units," *IET Renew. Power Gen.*, vol. 6, no. 5, pp. 303–314, Sep. 2012.
[21] H. E. Farag, M. M. A. Abdelaziz, and E. F. El-Saadany, "The effects of renewable energy resources on the implementation of distributed resources islanded systems," in *Proc. IEEE Power Energy Soc. General Meeting 2013,* Jul. 21–25, 2013, pp. 1–6.
[22] J. M. Guerrero, J. Matas, L. G. de Vicuna, M. Castilla, and J. Miret, "Decentralized control for parallel operation of distributed generation inverters using resistive output impedance," *IEEE Trans. Ind. Electron.*, vol. 52, no. 2, pp. 994–1004, Apr. 2007.
[23] W. Yao, M. Chen, J. Matas, J. M. Guerrero, and Z.-M. Qian, "Design and analysis of the droop control method for parallel inverters considering the impact of the complex impedance on the power sharing," *IEEE Trans. Ind. Electron.*, vol. 58, no. 2, pp. 576–588, Feb. 2011.
[24] K. De Brabandere, B. Bolsens, J. V. den Keybus, A. Woyte, J. Driesen, and R. Belmans, "A voltage and frequency droop control method for parallel inverters," *IEEE Trans. Power Electron.*, vol. 22, no. 4, pp. 1107–1115, Jul. 2007.
[25] Y. M. Atwa, E. F. El-Saadany, M. M. A. Salama, R. Seethapathy, M. Assam, and S. Conti, "Adequacy evaluation of distribution system including wind/solar DG during different modes of operation," *IEEE Trans. Power Syst.*, vol. 26, no. 4, pp. 1945–1952, Nov. 2011.
[26] A. Boring, R. Duisberg, B. Freeman-Benson, A. Kramer, and M. Woolf, "Constraint hierarchies," in *Proc. OOPSLA'87,* Oct. 1987, pp. 48–60.
[27] N. R. Ullah, K. Bhattacharya, and T. Thiringer, "Wind farms as reactive power ancillary service providers-technical and economic issues," *IEEE Trans. Energy Convers.*, vol. 24, no. 3, pp. 661–672, Sep. 2009.
[28] G. Diaz and C. Gonzalez-Moran, "Fischer-Burmeister-based method for calculating equilibrium points of droop-regulated microgrids," *IEEE Trans. Power Syst.*, vol. 27, no. 2, pp. 959–967, May 2012.
[29] W. Rosehart, C. Roman, and A. Schellenberg, "Optimal power flow with complementarity constraints," *IEEE Trans. Power Syst.*, vol. 20, no. 2, pp. 813–822, May 2005.
[30] R. S. Al Abri, E. F. El-Saadany, and Y. M. Atwa, "Optimal placement and sizing method to improve the voltage stability margin in a distribution system using distributed generation," *IEEE Trans. Power Syst.*, vol. 28, no. 1, pp. 326–334, Feb. 2013.
[31] W. Rosehart, C. Canizares, and V. H. Quintana, "Multiobjective optimal power flows to evaluate voltage security costs in power networks," *IEEE Trans. Power Syst.*, vol. 18, no. 2, pp. 578–587, May 2003.
[32] M. E. Baran and F. F. Wu, "Network reconfiguration in distribution systems for loss reduction and load balancing," *IEEE Trans. Power Del.*, vol. 4, no. 2, pp. 1401–1407, Apr. 1989.
[33] C. Singh and Y. Kim, "An efficient technique for reliability analysis of power systems including time dependent sources," *IEEE Trans. Power Syst.*, vol. 3, no. 3, pp. 1090–1096, Aug. 1989.

Morad Mohamed Abdelmageed Abdelaziz (S'11) was born in Cairo, Egypt, on September 27, 1984. He received the B.Sc. (with honors) and M.Sc. degrees from Ain Shams University, Cairo, Egypt, in 2006 and 2009, respectively, both in electrical engineering. He is currently working toward the Ph.D. degree in the Department of Electrical and Computer Engineering, University of Waterloo, Waterloo, ON, Canada.

He was an Electrical Design Engineer with Dar Al-Handasah Consultants (Shair and Partners), Cairo, Egypt, from 2006 to 2010, where he was engaged in projects involving distribution system design, and protection and distributed generation. His research interests include dynamics, controls, and analysis of microgrids and active distribution networks, and integration of distributed and renewable generation, power electronics converters, and their applications in smart grids.

Hany E. Farag (M'13) was born in Assiut, Egypt on November 21, 1982. He received the B.Sc. (with honors) and M.Sc. degrees in electrical engineering from Assiut University, Egypt, in 2004 and 2007, respectively, and the Ph.D. degree in electrical engineering from the University of Waterloo, Waterloo, ON, Canada, in 2013.

Currently, he is an Assistant Professor with the Department of Electrical Engineering and Computer Science, Lassonde School of Engineering, York University, Toronto, ON, Canada. His research interests are in the areas of active distribution networks, integration of distributed and renewable energy resources, modeling, analysis, and design of microgrids, and applications of multi-agent technologies in smart grids.

Dr. Farag's biography is listed in the 30th pearl anniversary edition of *Marquis Who's Who in the World* in 2012.

Ehab F. El-Saadany (SM'05) was born in Cairo, Egypt, in 1964. He received the B.Sc. and M.Sc. degrees in electrical engineering from Ain Shams University, Cairo, Egypt, in 1986 and 1990, respectively, and the Ph.D. degree in electrical engineering from the University of Waterloo, Waterloo, ON, Canada, in 1998.

Currently, he is a Professor with the Department of Electrical and Computer Engineering, University of Waterloo, Waterloo, ON, Canada. His research interests are smart grids operation and control, power quality, distributed generation, power electronics, digital signal processing applications to power systems, and mechatronics.

Authorized licensed use limited to: UNIV OF MIAMI LIB. Downloaded on May 27,2022 at 21:50:44 UTC from IEEE Xplore. Restrictions apply.